



## Plio-Pleistocene time-averaged field in southern Patagonia recorded in lava flows

**V. Mejia and N. D. Opdyke**

*Department of Geological Sciences, University of Florida, 241 Williamson Hall, P.O. Box 112120, Gainesville, Florida 32611-2120, USA (vmejia@ufl.edu; drno@ufl.edu)*

**J. F. Vilas**

*Departamento de Geología, Universidad de Buenos Aires, Ciudad Universitaria, Pabellon 2, Buenos Aires, 1428EHA, Argentina (vilas@gl.fcen.uba.ar)*

**B. S. Singer**

*Department of Geology and Geophysics, University of Wisconsin-Madison, 1215 West Dayton Street, Madison, Wisconsin 53706, USA (bsinger@geology.wisc.edu)*

**J. S. Stoner**

*INSTAAR, University of Colorado, 1560 30th Street, P.O. Box 450, Boulder, Colorado 80309-0450, USA (joseph.stoner@colorado.edu)*

[1] Paleomagnetic directions were obtained from stepwise alternating-field or thermal demagnetization of 53 lava flows from southern Patagonia (latitudes 49.5°–52.1°S) that include the Pali-Aike volcanic field and the Meseta Viscachas plateau lavas. In addition to previous Miocene-late Quaternary ages of these flows,  $^{40}\text{Ar}/^{39}\text{Ar}$  dates spanning from 0.1 to 15.4 Ma were obtained for 17 of the sites. All except one of the magnetic polarities coincide with the expected polarities of the magnetic polarity timescale [Cande and Kent, 1995] for the obtained  $^{40}\text{Ar}/^{39}\text{Ar}$  ages. The mean direction from 33 sites (eliminating sites  $\geq 4$  Ma) that pass a selection criteria of  $\alpha_{95} \leq 5^\circ$  is Dec = 358.7°, Inc = -68.2°,  $\alpha_{95} = 3.5^\circ$ , a value that coincides within the statistical uncertainty with the direction of the geocentric axial dipole for that area (Inc = -68.1°). Likewise, the mean virtual geomagnetic pole (VGP) coincides within the statistical uncertainty with the geographic North Pole. The secular variation described by the VGP angular standard deviation for these sites is 17.1°, a value expected for that latitude according to Model G of paleosecular variation [McFadden *et al.*, 1988]. The characteristics of the data presented are optimum for time-averaged field (TAF) studies because of the good age control and good quality of the paleomagnetic data: (1) primary components of magnetization were obtained using principal component analysis [Kirschvink, 1980] from at least five points and maximum angular deviation  $\leq 5^\circ$ , (2) site means were calculated with Fisher statistics using at least three samples, and (c) 38 of the 53 flows had  $\alpha_{95} \leq 5^\circ$ . No results (five sites) or high  $\alpha_{95}$  values ( $>5^\circ$ ) were obtained primarily from sites affected by lightning.

**Components:** 7325 words, 7 figures, 3 tables.

**Keywords:** paleomagnetic secular variation; Patagonia; Pali-Aike Volcanic Field; time-averaged field; lava flow; geocentric axial dipole.

**Index Terms:** 1522 Geomagnetism and Paleomagnetism: Paleomagnetic secular variation; 1560 Geomagnetism and Paleomagnetism: Time variations—secular and long term; 1530 Geomagnetism and Paleomagnetism: Rapid time variations.

**Received** 12 September 2003; **Revised** 20 January 2004; **Accepted** 20 January 2004; **Published** 2 March 2004.

Mejia, V., N. D. Opdyke, J. F. Vilas, B. S. Singer, and J. S. Stoner (2004), Plio-Pleistocene time-averaged field in southern Patagonia recorded in lava flows, *Geochem. Geophys. Geosyst.*, 5, Q03H08, doi:10.1029/2003GC000633.

**Theme:** Geomagnetic Field Behavior Over the Past 5 Myr **Guest Editors:** Cathy Constable and Catherine Johnson

## 1. Introduction

[2] The characteristics of the Earth's magnetic field in the present are well known from magnetic observatories and satellite, airplane, and ship data, but the history of the magnetic field blurs as we go into the past. The implementation of the magnetic compass in Europe by 1200 ultimately made possible historic records of the magnetic field. Compilations of historic records dating back to about 1600 have been used to model the magnetic field [Jackson *et al.*, 2000]. The Earth's magnetic field has also been modeled in other timescales such as the last 3000 years using archaeomagnetic data derived from pottery [Constable *et al.*, 2000] and in geologic times (the past 5 Myr) using paleomagnetic data derived from rock materials [e.g., Johnson and Constable, 1995] (hereinafter referred to as JC95). The analysis of these different kinds of records of the magnetic field has helped to understand both the time-averaged field (TAF) and its secular variation, which applied to the geologic past is referred to as paleosecular variation (PSV).

[3] Two main different archives of PSV are available: sediments and lavas. PSV obtained from the study of lava flows is generally referred to as PSVL. Lee [1983] compiled a paleomagnetic database from lavas of the past 5 Myr. This database has been subsequently updated by Quidelleur *et al.* [1994], Johnson and Constable [1996], and McElhinny and McFadden [1997]. After applying different selection criteria the number of records of the renovated databases is not much greater than the 2244 records in Lee's original compilation. The characteristics of any of these data sets are far from being ideal, the main deficiencies being that (1) the distribution over the Earth is not uniform, (2) most studies have been undertaken using paleomagnetic procedures that are now obsolete, and (3) age control is limited.

[4] A paleosecular variation study from two areas of southern Patagonia (latitudes 51.5° to 52.5°S and latitudes 49.5° to 50.5°S) is presented in this paper (Figure 1). The data will help to fill a gap of paleomagnetic data from high southern latitudes. The results that we obtained were compared with those predicted by existing TAF and PSVL models. The inclination anomalies depicted by some TAF models for this area (JC95) as well as the expected scatter of the virtual geomagnetic poles (VGPs) relative to the Earth's axis of rotation according to Model G of secular variation [McFadden *et al.*, 1988] are tested.

[5] We obtained samples from and around Meseta Viscachas (northern sampling area) and from the Pali-Aike volcanic field (Figure 1), the southernmost among a series of Late Cretaceous–Holocene alkali basaltic plateaus [Skewes and Stern, 1979] that extend east of the Patagonian Andes. Ramos and Kay [1992] have proposed that back arc volcanism in southern Patagonia is the result of slab window formation in the mantle produced by the collision of the Chile ridge with the South American plate. The tectonic environment in southernmost Patagonia is complicated by sinistral motion of the Scotia plate along the southwestern tip of Tierra del Fuego. Skewes and Stern [1979] suggest the presence of thermal or mechanical perturbations of the mantle related to the trench-transform triple junction between South American, Antarctic and Scotia plates, based on findings of ultramafic inclusions and chemical characteristics of the Pali-Aike basalts, that are indicative of a mantle origin and are not observed in other Patagonian plateau basalts.

[6] The Meseta Viscachas and Pali-Aike basaltic flows are locally interbedded with tills. K-Ar and <sup>40</sup>Ar/<sup>39</sup>Ar radioisotopic dates of these flows [Mercer, 1976; Meglioli, 1992; Singer *et al.*, 2004] obtained to help depict the glacial history in Patagonia indicate primarily Pliocene–Pleistocene

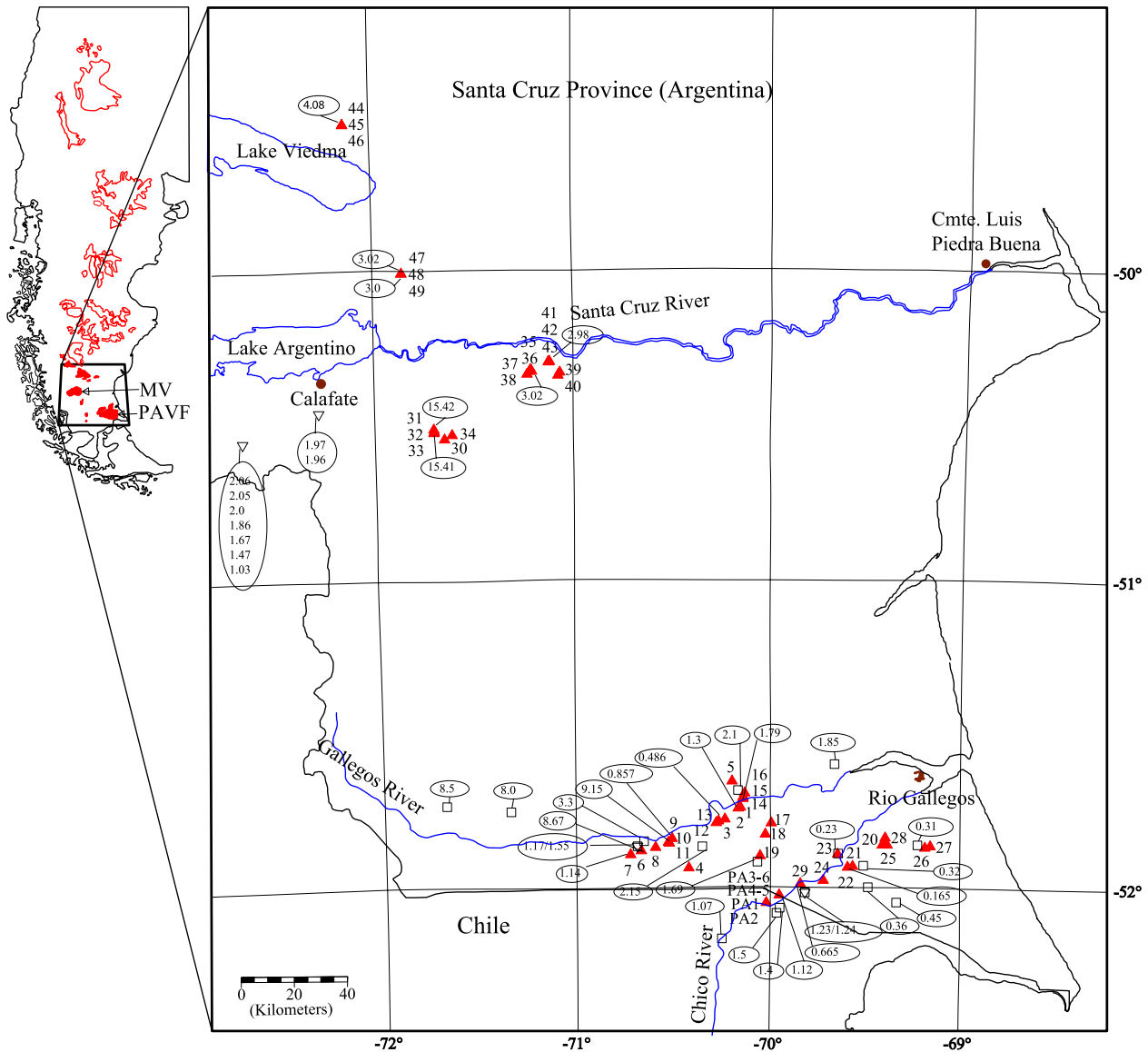


**Figure 1.** Location map of southern Patagonia showing sampling sites and radiometric dates obtained in this and previous studies. The general location map to the left (modified from *Skewes and Stern [1979]*) shows Upper Cretaceous to Quaternary alkali basaltic plateaus of Patagonia (red). The location of Meseta Viscachas and the Pali-Aike Volcanic field (red-fill areas) is designated as MV and PAVF, respectively. The map to the right contains the location of radiometric ( $^{40}\text{Ar}/^{39}\text{Ar}$ ) and/or paleomagnetic sampling sites (red-filled triangles pointing up). The sampling sites of previously obtained  $^{40}\text{Ar}/^{39}\text{Ar}$  [*Meglioli, 1992*] and K/Ar [*Mercer, 1976*] radiometric dates in the area are shown by squares and triangles pointing down, respectively. Results of radioisotopic dates (in Ma) are within ellipses.

ages. We obtained  $^{40}\text{Ar}/^{39}\text{Ar}$  radioisotopic dates from 17 of the paleomagnetic sites that support and complement previous results.

## 2. Sampling and Sampling Area

[7] Most of the samples (49 sites) were collected in Argentina during February of 2000. Four sites were

collected by Joe Stoner during February of 1998 in the Chilean part of the Pali-Aike volcanic field. Each site represents an individual lava flow. Access to the outcrops was achieved by road and tracks. Short hikes were occasionally necessary. Normally 10 samples were collected at each site and oriented using magnetic compass and sun compass. Sun compass declinations

were obtained for 75% of the collected samples and used for further calculations when they differed by 5° or more from the magnetic compass declinations. Two lava flows from the Chilean side of Patagonia were sampled twice and their data combined. This way, the pairs of sites PA3 and PA6 (PA3-6) and sites PA4 and PA5 (PA4-5) were combined.

### 2.1. Northern Sampling Area

[8] This region is adjacent to the Andes and consequently the relief is high. Lava flows east of the Andes are now often exposed in cliffs that have resulted from scarp retreat. Lava flows along these scarps outcrop in stratigraphic sequences composed usually of several (more than 3) flows.

### 2.2. Pali-Aike Volcanic Field

[9] The area sampled in the Pali-Aike volcanic field is predominantly flat and covered with Patagonian gravel. Some topography is created by lava flows and volcanic centers. We sampled lava flows, usually <10 m thick exposed in areas around and roughly along the eastern parts of the Rio Gallegos and Rio Chico valleys. In the area around Rio Gallegos, individual flows can be traced for a few kilometers, and up to three lava flows were sampled in stratigraphic order. Volcanic cones and eruptive centers are more eroded in the Rio Gallegos than in the Rio Chico area. In the Rio Chico area cinder cones (often aligned indicating fissure volcanism) are very well preserved. Examples of these cinder cones are Cerro de los Frailes, Cerro Conventos and Cerro Tres Hermanos. The geomorphologic differences between these two areas of the Pali-Aike volcanic field suggest that the lava flows that outcrop along Rio Gallegos are generally older than those that outcrop along Rio Chico, this is in agreement with results obtained from radioisotopic dating.

## 3. The $^{40}\text{Ar}/^{39}\text{Ar}$ Geochronology

[10] The  $^{40}\text{Ar}/^{39}\text{Ar}$  radioisotopic dating was carried out at the University of Wisconsin-Madison. Samples consisted of 50 mg of 180–500  $\mu\text{m}$  fraction of holocrystalline groundmass that were prepared by

crushing, sieving, magnetic sorting and picking under a binocular microscope. Samples were irradiated at the Oregon State University Triga reactor.  $^{40}\text{Ar}/^{39}\text{Ar}$  dating was applied using incremental heating technique. Ages were calculated relative to the  $1.94 \pm 0.012$  Ma Alder Creek Rhyolite sanidine that is intercalibrated to the  $28.34 \pm 0.16$  Ma Taylor Creek Rhyolite sanidine [Renne *et al.*, 1998]. The preferred ages were the isochron rather than the plateau ages. This way, no assumption is made about trapped argon and estimates of analytical precision and data scatter are considered. Our ages are about 0.6% older than the ages used by *Cande and Kent* [1995] to establish the geomagnetic polarity timescale (GPTS) because we have used updated ages of the argon standards. Further details about sample preparation as well as laboratory and data analysis are as described by *Singer et al.* [2002]. Table 1 contains a summary of results from 18  $^{40}\text{Ar}/^{39}\text{Ar}$  experiments.

## 4. Paleomagnetic Analysis

[11] Laboratory analysis was carried out in the paleomagnetic laboratory at the University of Florida. Alternating-field (AF) demagnetization was done using a Dtech D-200 AF demagnetizer and thermal demagnetization using a Schonstedt oven. Magnetic measurements were made in a 2G Cryogenic magnetometer in a shielded room. Pilot sets of samples composed of one sample per site and three samples per site were run using stepwise (around 17 steps) AF and thermal demagnetization, respectively to choose which method of demagnetization was more appropriate for each site. The general agreement between the directions obtained from AF and thermal demagnetization (Figures 2a and 2b) indicates that any CRM acquired during heating does not alter significantly the primary direction of magnetization, possibly due to low field conditions within the oven.

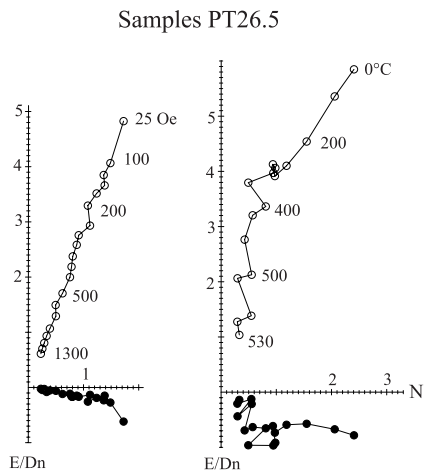
[12] Thermal demagnetization was the preferred procedure for processing all the samples from each site, except when the orthogonal projections from thermal demagnetization were more difficult to interpret than those from AF demagnetization (Figure 2a) or when the site was affected by

**Table 1.** Summary of  $^{40}\text{Ar}/^{39}\text{Ar}$  Incremental Heating Experiments

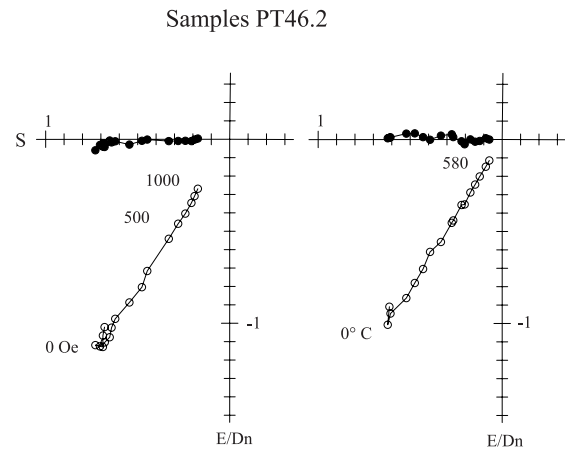
| Site     | Polarity | Groundmass |            |  | Age Spectrum                        |                    |                           |       | Isochron Analysis |            |   |  |
|----------|----------|------------|------------|--|-------------------------------------|--------------------|---------------------------|-------|-------------------|------------|---|--|
|          |          | wt., mg    | K/Ca Total | Total Fusion Age, Ma ( $\pm 2\sigma$ ) | Increments Used, $^{\circ}\text{C}$ | $^{39}\text{Ar}\%$ | Age, Ma ( $\pm 2\sigma$ ) | MSWD  | Steps N           | SUMS (N-2) | $^{40}\text{Ar}/^{36}\text{Ar}_i$ ( $\pm 2\sigma$ ) | Age, Ma <sup>a</sup> ( $\pm 2\sigma$ ) |
|          |          |            |            |  |                                     |                    |                           |       |                   |            |   |  |
| PT-22    | N        | 50         | 0.138      | 0.181 $\pm$ 0.015                      | 800–1250                            | 98.3               | 0.175 $\pm$ 0.018         | 2.04  | 7 of 9            | 2.01       | 296.7 $\pm$ 5.3                                     | 0.165 $\pm$ 0.046                      |
| PT-13    | N        | 50         | 0.108      | 0.543 $\pm$ 0.061                      | 1100–1350                           | 57.3               | 0.495 $\pm$ 0.038         | 0.02  | 3 of 6            | 0.00       | 296.0 $\pm$ 4.9                                     | 0.486 $\pm$ 0.096                      |
| PT-29    | N        | 50         | 0.118      | 0.473 $\pm$ 0.037                      | 1000–1250                           | 52.1               | 0.617 $\pm$ 0.053         | 1.69  | 5 of 14           | 2.01       | 291.1 $\pm$ 15.2                                    | 0.665 $\pm$ 0.168                      |
| PT-9     | R        | 50         | 0.538      | 0.916 $\pm$ 0.025                      | 775–1030                            | 52.8               | 0.849 $\pm$ 0.020         | 1.05  | 8 of 14           | 1.16       | 294.0 $\pm$ 4.3                                     | 0.857 $\pm$ 0.032                      |
| PA-3     | N        | 50         | 0.194      | 1.102 $\pm$ 0.011                      | 1225–1400                           | 49.4               | 1.113 $\pm$ 0.010         | 1.25  | 3 of 6            | 1.00       | 294.1 $\pm$ 2.235                                   | 1.12 $\pm$ 0.01                        |
| PT-7     | R        | 50         | 0.137      | 1.13 $\pm$ 0.02                        | 600–1250                            | 100.0              | 1.13 $\pm$ 0.01           | 0.84  | 10 of 10          | 0.49       | 293.4 $\pm$ 2.2                                     | 1.14 $\pm$ 0.02                        |
| PT-2     | R        | 50         | 0.876      | 1.30 $\pm$ 0.03                        | 925–1075                            | 47.2               | 1.31 $\pm$ 0.02           | 0.63  | 3 of 9            | 1.25       | 295.9 $\pm$ 8.1                                     | 1.30 $\pm$ 0.03                        |
| PT-14    | R        | 50         | 0.155      | 1.68 $\pm$ 0.03                        | 925–1250                            | 72.8               | 1.67 $\pm$ 0.03           | 1.17  | 7 of 12           | 0.71       | 276.3 $\pm$ 19.7                                    | 1.79 $\pm$ 0.12                        |
| PT-41    | N        | 50         | 0.085      | 2.96 $\pm$ 0.03                        | 875–1120                            | 98.6               | 2.98 $\pm$ 0.03           | 1.10  | 5 of 7            | 1.13       | 294.5 $\pm$ 2.2                                     | 2.98 $\pm$ 0.03                        |
| PT-49    | N        | 50         | 0.258      | 2.91 $\pm$ 0.03                        | 950–1050                            | 53.7               | 3.01 $\pm$ 0.03           | 0.29  | 3 of 11           | 0.23       | 296.5 $\pm$ 3.6                                     | 3.00 $\pm$ 0.04                        |
| PT-37    | N        | 50         | 0.254      | 3.01 $\pm$ 0.03                        | 725–1060                            | 91.7               | 3.04 $\pm$ 0.03           | 1.23  | 6 of 8            | 1.01       | 297.1 $\pm$ 2.2                                     | 3.02 $\pm$ 0.04                        |
| PT-47    | N        | 50         | 0.225      | 3.00 $\pm$ 0.03                        | 1000–1250                           | 71.8               | 3.02 $\pm$ 0.03           | 1.38  | 5 of 11           | 0.49       | 289.9 $\pm$ 5.4                                     | 3.02 $\pm$ 0.03                        |
| PT-44/45 | R        | 50         | 0.660      | 3.39 $\pm$ 0.19                        | 940–1090                            | 57.1               | 4.00 $\pm$ 0.06           | 2.49  | 6 of 14           | 1.92       | 287.6 $\pm$ 9.9                                     | 4.08 $\pm$ 0.12                        |
| PT-6     | R        | 50         | 0.051      | 8.01 $\pm$ 0.13                        | 1000–1450                           | 80.7               | 8.62 $\pm$ 0.11           | 0.46  | 5 of 9            | 0.24       | 293.8 $\pm$ 3.1                                     | 8.67 $\pm$ 0.15                        |
| PT-11 gm | N        | 50         | 0.546      | 9.06 $\pm$ 0.05                        | 1000–1275                           | 91.0               | 9.10 $\pm$ 0.06           | 1.62  | 3 of 5            | 1.10       | 281.1 $\pm$ 20.5                                    | 9.15 $\pm$ 0.08                        |
| PT-11 wr | N        | 100        | 0.521      | 9.18 $\pm$ 0.06                        | 925–1040                            | 87.3               | 9.25 $\pm$ 0.06           | 0.16  | 3 of 5            | 0.25       | 308.9 $\pm$ 101.7                                   | 9.22 $\pm$ 0.27                        |
| PT-31    | I        | 50         | 0.353      | 15.26 $\pm$ 0.15                       | 975–1250                            | 85.4               | 15.35 $\pm$ 0.16          | 2.71* | 7 of 13           | 1.30       | 285.6 $\pm$ 9.4                                     | 15.42 $\pm$ 0.17                       |
| PT-32    | R        | 50         | 0.029      | 15.35 $\pm$ 0.16                       | 700–1250                            | 100.0              | 15.39 $\pm$ 0.16          | 0.82  | 9 of 9            | 0.60       | 293.2 $\pm$ 3.0                                     | 15.41 $\pm$ 0.16                       |

<sup>a</sup> Ages calculated relative to 1.194 Ma Alder Creek Rhyolite sanidine [Renne *et al.*, 1998]; uncertainties are greater than those due to analytical errors [Singer *et al.*, 2002].

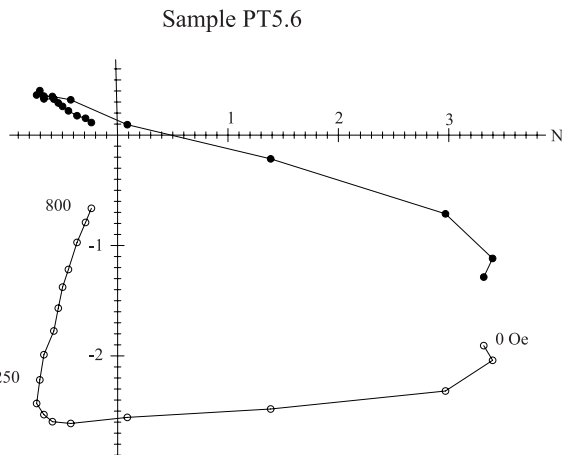
a)



b)



c)



d)

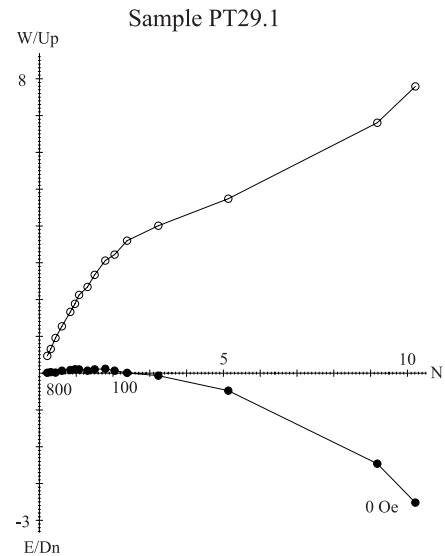


**Figure 2.** Examples of Zijderveld diagrams. Figures 2a and 2b are AF and thermal demagnetization (left and right, respectively) on replicate samples. Figure 2a shows a case in which the thermal demagnetization curve is difficult to interpret and the AF demagnetization curve is not, while both methods still indicate the same general direction. Figure 2b is an example of both AF and thermal demagnetization curves showing similar results and Figures 2c and 2d show demagnetization curves of sites affected by lightning. Approximate intensity values are in A/m.

lightning (Figures 2c and 2d). The most distinctive symptoms of sites being affected by lightning are scatter in directions and high intensity of the NRM (reaching around 20 A/m in some of the samples whereas the intensity of magnetization of the sites not affected by lightning is around 4 A/m). Twelve of our sites showed signs of being affected by

lightning; therefore we applied AF demagnetization, which is the most successful method to remove the overprint caused by lightning-induced IRM. The remaining 20 sites that were treated using AF demagnetization were those in which the thermal treatment produced a noisy orthogonal projection or rapid loss of most of the magnetiza-

tion during the first few temperature steps, while results from AF demagnetization were clear. Other researchers have also documented more successful AF versus thermal demagnetization treatments on basaltic flows [e.g., *Camps et al.*, 2001; *Szeremeta et al.*, 1999]. Despite the preference to apply thermal demagnetization, AF demagnetization was used more times (in 32 sites) than thermal demagnetization (in 21 sites).

## 5. Data Analysis and Selection Criteria

[13] The procedures to obtain and process paleomagnetic data were aimed at obtaining high quality results. We followed the procedures and selection criteria for data analysis used by *Tauxe et al.* [2000]. That is, the primary component of magnetization from individual samples was obtained using principal component analysis [*Kirschvink*, 1980] from a segment of at least 5 points of the orthogonal projection directed toward the origin and with maximum angular deviation  $\leq 5^\circ$ . Site mean directions were calculated from at least 3 samples per site using *Fisher* [1953] statistics and selected as successful when  $\alpha_{95}$  values were  $\leq 5^\circ$  (rounded to the nearest integer).

[14] A summary of the paleomagnetic results of all the sites is contained in Table 2 and the data plotted in Figures 3 and 4a. We obtained successful paleomagnetic results from most of the sites (except site PA1) that were treated using thermal demagnetization. AF demagnetization was applied to 32 sites. Among the 12 sites treated using AF demagnetization, as an alternative for treating samples affected by lightning, 4 sites had random directions (no results), 6 sites had  $\alpha_{95}$  values  $> 5^\circ$  and only 2 sites had  $\alpha_{95} \leq 5^\circ$ , complying with our selection criteria. Among the remaining 20 sites that were treated using AF demagnetization only 4 sites did not pass the selection criteria.

[15] Many of the sites that were rejected occupy the periphery of the overall distribution of paleomagnetic directions (Figure 3), which suggests that the applied selection criteria are successfully filtering out noise in the paleomagnetic data. Likewise the application of detailed stepwise demagnetization seems to improve the quality of the data.

Previous paleomagnetic analysis by *Fleck et al.* [1972] in a sequence of lava flows interbedded with tills from Cerro El Fraile (south of Lago Argentino), that used mild or no demagnetization techniques, rendered results with  $\alpha_{95}$  values higher than  $10^\circ$ , that do not pass our selection criteria.

## 6. Radioisotopic Ages

[16] The radioisotopic dates that we obtained from 17 of the 53 paleomagnetic sites sampled indicate mostly Pliocene–Pleistocene ages. *Mercer* [1976], *Meglioli* [1992], and *Singer et al.* [2004] have obtained similar results (Figure 1 and Tables 1 and 2). Table 1 shows a summary of the radioisotopic results obtained in this study where analytical uncertainty is reported as  $2\sigma$ . The preferred ages (isochrons) are also shown in Table 2. Figure 5 shows two examples of age spectra and isochrons.

### 6.1. Northern Sampling Area

[17] Seven of the 20 sites in this area were dated. In all cases the magnetic polarities coincided with the ones expected from the magnetic polarity timescale [*Cande and Kent*, 1995]. Flows PT31 and PT32 with reverse polarity were dated at 15.4 Ma. These two flows were not considered for the calculation of mean directions or mean VGPs, because their ages are out of the scope of this study. The nearby flows PT33 (a dyke with intermediate direction), PT34 and PT30 located close to the previously mentioned sites were not considered either, because of lack of age control. The isochron ages of the remaining dated flows in this area indicated either Gauss or Gilbert magnetic chrons (spanning from 2.98 to 4.08 Ma) in agreement with previously dated nearby sites [*Mercer*, 1976]. Most of the sites that were not dated crop out in stratigraphic sequences in which at least one of the flows was dated. In these cases we assumed for the undated flows the magnetic chron obtained for the dated lava flow in that sequence, provided that the same polarity was observed among all lava sequences. The only stratigraphic sequence in which no lava flow was radioisotopically dated was that composed of flows PT39 and PT40. Because of their normal polarity and closeness to flows PT41 (determined as Gauss) they probably

**Table 2.** Summary of Paleomagnetic Results<sup>a</sup>

| Site  | U/L | Site   |        | Dec   | Inc   | SC | N     | $\alpha_{95}$<br>Dir | K<br>Dir | Th/<br>AF | L | VGP   |       | $\alpha_{95}$<br>VGP | K<br>VGP | R.D., |             | R |
|-------|-----|--------|--------|-------|-------|----|-------|----------------------|----------|-----------|---|-------|-------|----------------------|----------|-------|-------------|---|
|       |     | Lat    | Long   |       |       |    |       |                      |          |           |   | Lat   | Long  |                      |          | Ma    | U ( $\pm$ ) |   |
| PT1   |     | -51.74 | -70.15 | -     | -     | 9  | 0/9   | -                    | -        | AF        |   |       |       |                      |          | -     | -           | - |
| PT2   |     | -51.74 | -70.17 | 140.8 | 64.7  | 0  | 6/10  | 14.4                 | 22       | AF        | X | -64.1 | 9.9   | 17.9                 | 15       | 1.3   | 0.03        | a |
| PT3   |     | -51.78 | -70.23 | 357.1 | -65.7 | 9  | 8/9   | 3.7                  | 231      | Th        |   | 86    | 263   | 5.5                  | 103      |       |             |   |
| PT4   |     | -51.94 | -70.42 | 142   | 60.5  | 0  | 7/10  | 3.2                  | 368      | Th        |   | -62.4 | 26.4  | 4.1                  | 216      |       |             |   |
| PT5   |     | -51.68 | -70.19 | 196.7 | 66.0  | 0  | 5/10  | 4.7                  | 264      | AF        | X | -78.7 | 189.9 | 7.4                  | 107      |       |             |   |
| PT6   |     | -51.88 | -70.66 | 217.7 | 59.0  | 0  | 10/10 | 1.4                  | 1202     | Th        |   | -61.6 | 189.4 | 1.8                  | 721      | 8.67  | 0.15        | a |
| PT7   |     | -51.89 | -70.72 | 186.4 | 60.4  | 9  | 8/9   | 2.3                  | 605      | AF        |   | -78.6 | 134.4 | 3.2                  | 302      | 1.14  | 0.02        | a |
| PT8   |     | -51.87 | -70.59 | 185.4 | 60.7  | 8  | 7/8   | 4                    | 229      | AF        |   | -79.2 | 132.2 | 5.8                  | 108      |       |             |   |
| PT9   |     | -51.84 | -70.51 | 183.4 | 71    | 10 | 4/10  | 7.1                  | 167      | AF        | X | -85.4 | 264.4 | 10.8                 | 73       | 0.857 | 0.032       | a |
| PT10  |     | -51.85 | -70.52 | 172.9 | 76.5  | 10 | 10/10 | 2.4                  | 391      | Th        |   | -76.9 | 302.8 | 4.3                  | 129      |       |             |   |
| PT11  |     | -51.86 | -70.52 | 4.5   | -57.1 | 11 | 9/11  | 3.4                  | 235      | AF        |   | 75.7  | 303.9 | 4.1                  | 158      | 9.16  | 0.08        | a |
| PT12  |     | -51.79 | -70.28 | 184.6 | 60.3  | 10 | 3/10  | 12                   | 107      | AF        | X | -79.2 | 130.2 | 16.8                 | 55       |       |             |   |
| PT13  |     | -51.78 | -70.27 | 355.8 | -71.7 | 10 | 10/10 | 2.4                  | 400      | Th        |   | 84.6  | 134.8 | 4.1                  | 142      | 0.486 | 0.096       | a |
| PT14  | L   | -51.72 | -70.15 | 200.5 | 68.4  | 11 | 9/11  | 4.3                  | 147      | AF        |   | -77.4 | 209.2 | 6.6                  | 63       | 1.79  | 0.12        | a |
| PT15  |     | -51.72 | -70.15 | 170.4 | 54.4  | 1  | 5/11  | 3.3                  | 537      | AF        |   | -71.9 | 83.8  | 4.2                  | 326      |       |             |   |
| PT16  | U   | -51.71 | -70.15 | 150.2 | 72.6  | 7  | 6/10  | 5.5                  | 149      | AF        |   | -71.7 | 346.3 | 8.5                  | 63       |       |             |   |
| PT17  |     | -51.79 | -70.00 | -     | -     | 10 | 0/10  | -                    | -        | AF        | X |       |       |                      |          | -     | -           |   |
| PT18  |     | -51.83 | -70.03 | -     | -     | 0  | 0/10  | -                    | -        | AF        | X |       |       |                      |          | -     | -           |   |
| PT19  |     | -51.90 | -70.05 | 356   | -76.5 | 0  | 9/10  | 3.5                  | 222      | AF        |   | 77.3  | 117.2 | 6.2                  | 69       | 0.69  | 0.05        | b |
| PT20  |     | -51.87 | -69.42 | 30.3  | -37.6 | 6  | 5/10  | 8.7                  | 79       | AF        | X | 51.5  | 339.9 | 6.2                  | 155      |       |             |   |
| PT21  |     | -51.94 | -69.57 | 352.2 | -73   | 10 | 7/10  | 2.7                  | 513      | AF        |   | 82    | 140.7 | 4.6                  | 175      | 0.32  | 0.02        | b |
| PT22  |     | -51.94 | -69.60 | 342   | -65.7 | 10 | 7/9   | 3.9                  | 244      | AF        |   | 78    | 211.3 | 5.6                  | 116      | 0.165 | 0.046       | a |
| PT23  |     | -51.91 | -69.64 | 295.8 | -81.8 | 0  | 7/10  | 4.5                  | 184      | AF        |   | 56.4  | 136.7 | 8.4                  | 53       | 0.23  | 0.02        | b |
| PT24  |     | -51.98 | -69.73 | 351.6 | -57.8 | 9  | 9/10  | 4.4                  | 140      | AF        |   | 75.7  | 263.4 | 5.1                  | 102      |       |             |   |
| PT25  |     | -51.87 | -69.39 | 43.2  | -51.7 | 0  | 3/10  | 8.2                  | 226      | AF        | X | 53.4  | 5.7   | 8.7                  | 201      |       |             |   |
| PT26  |     | -51.88 | -69.19 | 18.1  | -73.3 | 10 | 10/10 | 3.7                  | 174      | AF        |   | 77.4  | 63.5  | 6.4                  | 58       | 0.31  | 0.03        | b |
| PT27  |     | -51.87 | -69.17 | 10.4  | -72   | 11 | 11/11 | 3.6                  | 163      | AF        |   | 81.8  | 66.2  | 5.8                  | 62       | 0.31  | 0.03        | b |
| PT28  |     | -51.84 | -69.40 | -     | -     | 10 | 0/10  | -                    | -        | AF        | X |       |       |                      |          | -     | -           |   |
| PT29  |     | -51.99 | -69.85 | 350.7 | -63.6 | 10 | 6/10  | 5                    | 179      | AF        | X | 80.9  | 242.7 | 7.2                  | 87       | 0.665 | 0.168       | a |
| PT30  |     | -50.55 | -71.65 | 317.8 | -75.8 | 9  | 8/10  | 2.8                  | 386      | Th        |   | 64.4  | 152.5 | 4.7                  | 142      |       |             |   |
| PT31  |     | -50.52 | -71.70 | -     | -     | 10 | 0/10  | -                    | -        | AF        |   |       |       |                      |          | 15.42 | 0.17        | a |
| PT32  |     | -50.52 | -71.70 | 180.4 | 63.1  | 10 | 10/10 | 2.1                  | 512      | Th        |   | -84.1 | 111   | 3                    | 253      | 15.41 | 0.16        | a |
| PT33  |     | -50.52 | -71.70 | 49.2  | 49.1  | 10 | 10/10 | 4.6                  | 113      | Th        |   | -1.6  | 329.3 | 5.8                  | 69       |       |             |   |
| PT34  |     | -50.53 | -71.61 | 297.9 | -77.6 | 10 | 6/10  | 9.7                  | 49       | AF        |   | 56.3  | 144.6 | 15.2                 | 20       |       |             |   |
| PT35  | *   | -50.32 | -71.22 | 44.2  | -70.6 | 10 | 6/10  | 4.5                  | 221      | Th        |   | 63.5  | 46.3  | 7.2                  | 87       |       |             |   |
| PT36  | U   | -50.32 | -71.22 | 24.8  | -63.7 | 9  | 8/10  | 2.9                  | 366      | Th        |   | 72.8  | 12.1  | 4.2                  | 179      |       |             |   |
| PT37  | L   | -50.32 | -71.21 | 11.7  | -66.5 | 10 | 6/10  | 5.9                  | 131      | AF        |   | 82.7  | 15.2  | 8.9                  | 58       | 3.02  | 0.04        | a |
| PT38  |     | -50.34 | -71.23 | 34.5  | -65.4 | 5  | 6/9   | 6.9                  | 95       | AF        | X | 67.5  | 25.2  | 10.7                 | 40       |       |             |   |
| PT39  | L   | -50.33 | -71.07 | 8.2   | -74.2 | 10 | 7/10  | 3.4                  | 312      | AF        |   | 78.7  | 88.3  | 5.9                  | 107      |       |             |   |
| PT40  | U   | -50.34 | -71.07 | 6.3   | -79.2 | 10 | 9/10  | 4.6                  | 126      | AF        |   | 71.1  | 102.7 | 8.4                  | 39       |       |             |   |
| PT41  | U   | -50.29 | -71.13 | 38.4  | -72.5 | 0  | 6/11  | 2.2                  | 912      | Th        |   | 66.7  | 52.5  | 3.7                  | 336      | 2.98  | 0.03        | a |
| PT42  |     | -50.29 | -71.13 | 27.2  | -67.8 | 6  | 5/9   | 3.6                  | 462      | AF        |   | 72.7  | 31.4  | 5.8                  | 174      |       |             |   |
| PT43  | L   | -50.29 | -71.12 | -     | -     | 1  | 0/9   | -                    | -        | AF        | X |       |       |                      |          | -     | -           |   |
| PT44  | L   | -49.51 | -72.13 | 179.3 | 52.8  | 10 | 10/10 | 1.8                  | 694      | Th        |   | -73.9 | 105.8 | 2.1                  | 554      | 4.08  | 0.12        | a |
| PT45  |     | -49.51 | -72.13 | 180   | 58.3  | 10 | 9/10  | 2.9                  | 308      | Th        |   | -79.6 | 108.4 | 3.8                  | 181      |       |             |   |
| PT46  | U   | -49.51 | -72.13 | 184.3 | 56.9  | 10 | 9/10  | 2.3                  | 495      | Th        |   | -77.6 | 123.7 | 3.2                  | 254      |       |             |   |
| PT47  | L   | -50.01 | -71.87 | 345.3 | -66.3 | 8  | 7/10  | 3                    | 408      | Th        |   | 80.4  | 199.6 | 4.3                  | 199      | 3.02  | 0.03        | a |
| PT48  |     | -50.01 | -71.87 | 352.4 | -74.1 | 11 | 10/11 | 4.2                  | 130      | Th        |   | 78.1  | 126.9 | 7                    | 49       |       |             |   |
| PT49  | U   | -50.01 | -71.87 | 342.2 | -67.4 | 10 | 9/10  | 1.5                  | 1129     | Th        |   | 79    | 190.2 | 2.2                  | 536      | 3     | 0.04        | a |
| PA1   |     | -52.05 | -70.02 | 31.9  | -61.9 | 0  | 4/4   | 17.3                 | 29       | Th        |   | 67    | 10.4  | 26.1                 | 13       |       |             |   |
| PA2   |     | -52.05 | -70.02 | 26.2  | -51.9 | 6  | 5/8   | 4                    | 358      | Th        |   | 62.9  | 344.3 | 4.7                  | 267      |       |             |   |
| PA3-6 | L   | -52.02 | -69.93 | 323.7 | -62.0 | 17 | 13/17 | 2.5                  | 271      | Th        |   | 64.4  | 205.2 | 3.5                  | 139      | 1.12  | 0.01        | a |
| PA4-5 | U   | -52.02 | -69.93 | 315   | -65.1 | 19 | 17/19 | 1.8                  | 404      | Th        |   | 61.4  | 192   | 2.5                  | 204      |       |             |   |

<sup>a</sup>U/L indicates the uppermost and lowermost lava flows of lava sequences; the asterisk in site 35 indicates that it is in between the following two sites. Dec and Inc are the mean site declination and inclination; SC is the number of sun compass declinations obtained in each site; n/N is the number of samples used for calculation of site-mean direction per number of processed samples. K is the dispersion parameter of directions (Dir) or VGPs;  $\alpha_{95}$  is the 95% confidence cone about the mean direction (Dir) or mean VGP; Th/AF represent mean direction results after thermal or AF demagnetization; R.D. is the <sup>40</sup>Ar/<sup>39</sup>Ar radioisotopic date obtained for some sites; U is the uncertainty range of the radioisotopic date. R is the reference source on which a given radioisotopic date is based: (a) is this study and (b) is *Meglioli* [1992]. Sites PA1, PA2, PA3, PA4, PA5, and PA6 were labeled on the samples as BN1, BN2, SDL1, SDU1, SDU2, and SDL2, respectively.

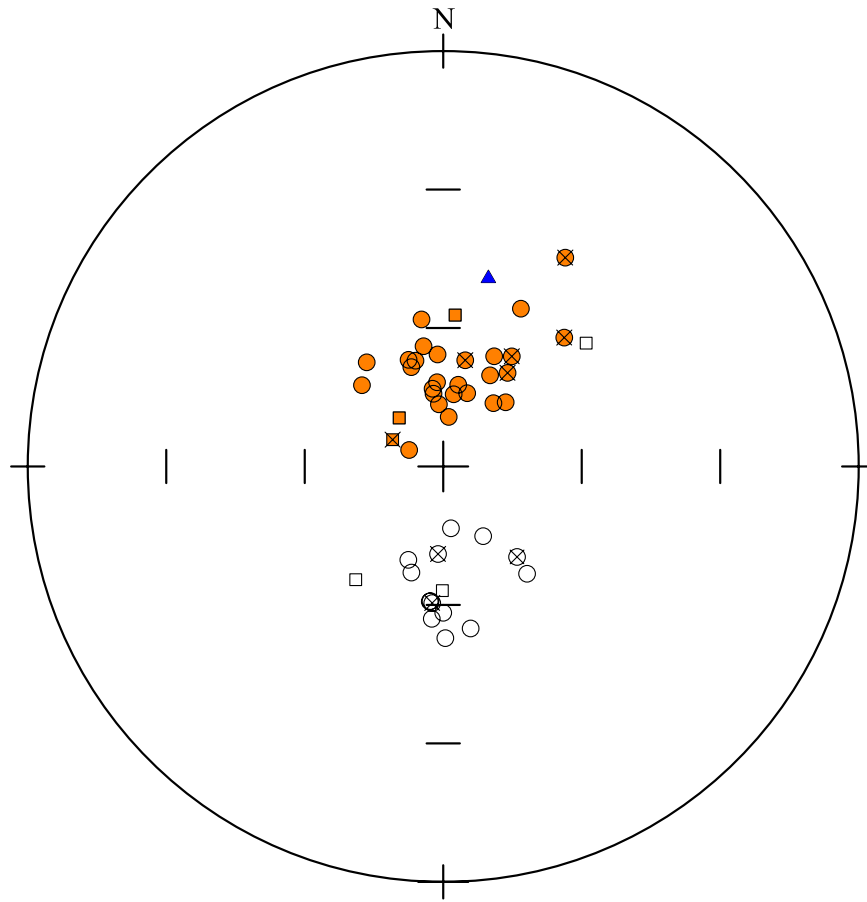


**Figure 3.** Equal area projection of site mean directions. The figure shows site mean directions of sites thought to be Plio-Pleistocene in age (circles) and of Miocene or unconstrained ages (squares). Magnetic vectors pointing up and down are represented by shaded and unshaded areas, respectively; crossed sites are rejected sites because of the quality of the paleomagnetic data. The IGRF (blue triangle) is plotted as a reference point.

correspond to the Gauss polarity chron. The nearby site PT38 is not discussed because paleomagnetic results were considered unsuccessful for this site.

## 6.2. Pali-Aike Volcanic Field

[18] Ten of the 33 sites of this area were dated. The radioisotopic dates that we obtained range from 9.15 Ma to 0.165 Ma. This age range is similar to that indicated by previous radiometric dates (*Mercher, 1976; Meglioli, 1992* and *Singer et al., in press*) in this volcanic field (Figure 1). The radioisotopic age obtained for site PT11 was checked and confirmed by a second measurement using whole rock material (Table 1). The initial result was preferred for being more precise and the product of a measurement of groundmass material. Site PT24 corresponds to a lava flow that has not been covered by soil that

according to *Skewes and Stern [1979]* represents the most recent volcanic activity in the Pali-Aike volcanic field that took place 5000 to 10000 yr B.P., based on anthropologic studies [*Bird, 1938*]. In all but one case the magnetic polarities that we obtained for the dated lava flows were in agreement with those expected from their ages, according to the magnetic polarity timescale [*Cande and Kent, 1995*]. Despite its lack of coincidence with the magnetic polarity timescale, the normal polarity of site PA3-6 (isochron age of  $1.12 \pm 0.01$  Ma) does coincide with the Punaruu Event [*Singer et al., 1999*] with a recalculated age of  $1.12 \pm 0.01$  Ma [*Singer et al., 2002*].

[19] The northern part of the Pali-Aike volcanic field, along Gallegos river has two flows with radioisotopic dates  $\geq 8.67$  Ma (PT6 and PT11) that

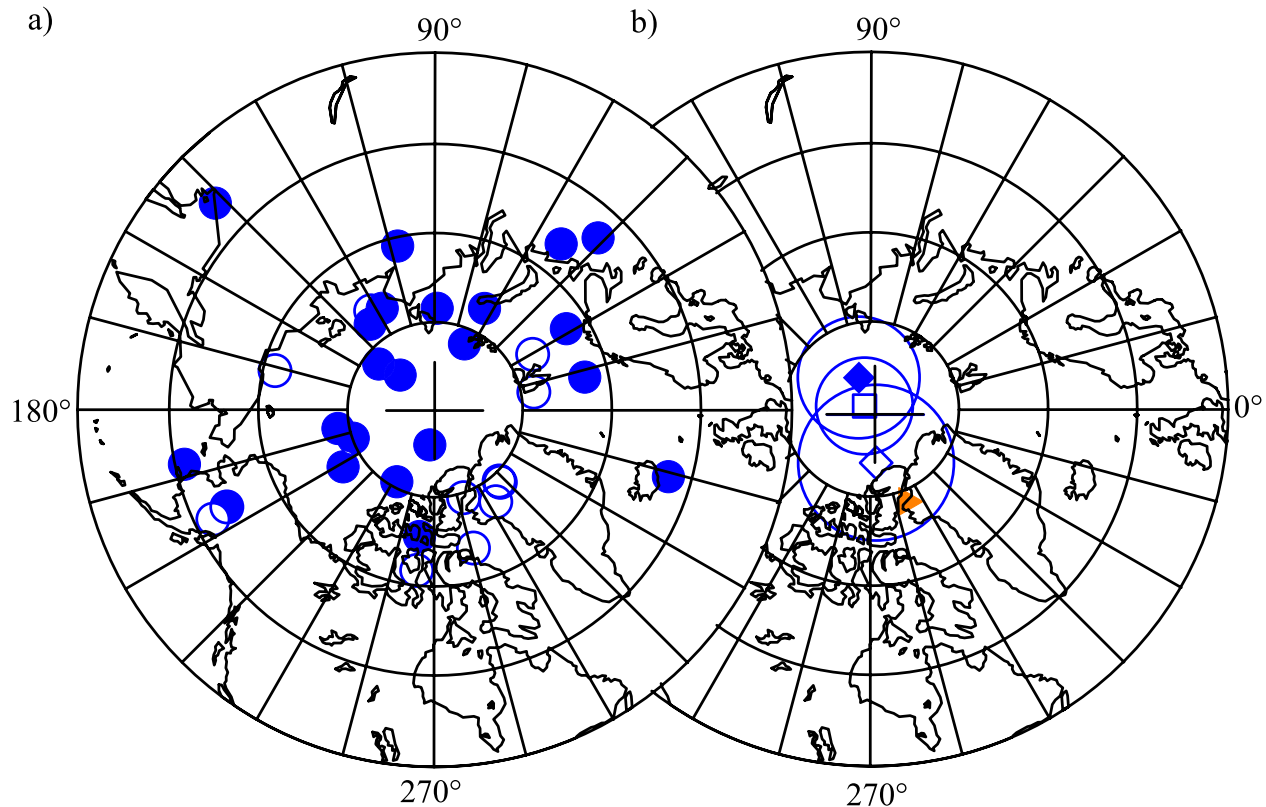


**Figure 4.** Paleomagnetic results expressed in VGPs. Magnetic vectors pointing up and down are represented by shaded and unshaded areas respectively. (a) Site-mean VGPs and (b) Mean VGP from selected group of sites (square), normal sites (filled diamond) and reversed sites (empty diamond). Triangle indicates the position of the geomagnetic North Pole.

occupy relatively high elevations and are remnants of old lava flows. Similar ages were obtained by *Meglioli* [1992] around 80 km west of these sites (Figure 1). These two flows were excluded for the calculation of mean directions or mean VGPs in order to focus the analysis on Pliocene-Pleistocene lava flows. All the other sites that were dated in the Pali-Aike volcanic field are less than 1.79 Ma. The remaining sites that were not dated in this volcanic field were considered for paleomagnetic analysis. A Pliocene-Pleistocene age was assumed for some of the undated flows by (1) inferring a similar age of that of a dated flow within the same lava sequence (such is the case of flows PT15 and PT16 that are assumed to have a similar age of flow PT14); (2) inferring a young age when the sampled lava correspond to a volcanic structure (such is the case of flow PT3, PT10, PT20 and PT25), and (3) inferring a similar age of a previously obtained nearby radioisotopic date (Figure 1)

like in the case of the flows related to cinder cones that crop out roughly along Rio Chico (sites PT21, PT23, PT26 and PT27). A relationship of sites PT5 and PT19 with previous nearby radiometric dates of 2.1 Ma and 0.69 Ma, respectively [*Meglioli*, 1992] is more difficult to determine due to the relative greater distance and the complex stratigraphic relations of the lava flows in the area. The previously mentioned two flows along with the undated flows PT4, PT8 and PT12 were considered for calculation of mean directions and mean VGPs, despite that there is some possibility that these flows are older than Pliocene in age.

## 7. Results

[20] No attempt was made to filter the data of serial correlation in lava sequences, considering the contention of *Love* [2000] that this procedure can be inadequate due to the possibility of slow secular

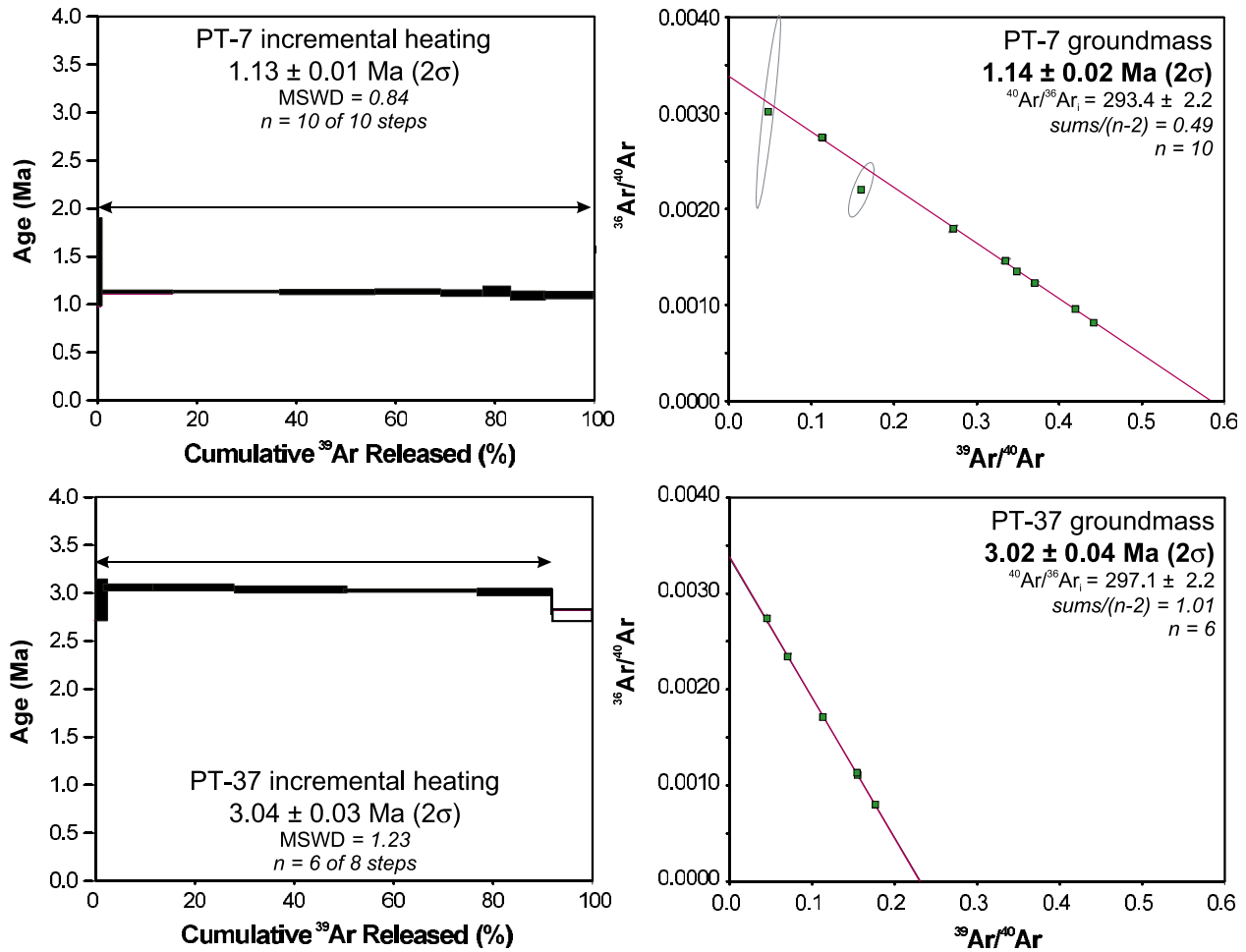


Figure 5. Examples of selected age spectra and isochrons.

variation of the magnetic field rather than fast accumulation rate of lava flows. However, the only flows in lava sequences that have overlapping circles of confidence are flows PT45-PT46, PT39-PT40 and PA3-6 - PA4-5.

[21] Table 3 summarizes mean directions and mean VGPs among groups of sites calculated using the statistical methods of Fisher [1953]. According to the selection criteria previously described we obtained 38 successful paleomagnetic results out

Table 3. Statistical Data Among Groups of Sites<sup>a</sup>

| Group of Sites      | Dec   | Inc   | N  | VGP               |       |          |       |       |                   |       | O.G. | O.A. | S <sub>t</sub> | S <sub>b</sub> | S <sub>u</sub> | S <sub>l</sub> |          |
|---------------------|-------|-------|----|-------------------|-------|----------|-------|-------|-------------------|-------|------|------|----------------|----------------|----------------|----------------|----------|
|                     |       |       |    | $\alpha_{95}$ Dir | K Dir | Fish Dir | Long  | Lat   | $\alpha_{95}$ VGP | K VGP |      |      |                |                |                |                | Fish VGP |
| Selected            | 358.7 | -68.2 | 33 | 3.5               | 51    | yes      | 141.3 | 88.5  | 5.4               | 22    | yes  | yes  | yes            | 17.3           | 17.1           | 20.6           | 14.6     |
| Selected + rejected | 3.3   | -67.3 | 41 | 3.6               | 40    | yes      | 24.5  | 88.2  | 5.3               | 19    | yes  | yes  | yes            | 18.9           | 18.6           | 21.9           | 16.6     |
| Normal              | 359.3 | -70.6 | 22 | 4.3               | 53    | yes      | 113.8 | 85.5  | 6.8               | 22    | yes  | yes  | yes            | 18.2           | 18.0           | 22.6           | 14.9     |
| Reverse             | 177.7 | 63.4  | 11 | 6.1               | 57    | yes      | 91.3  | -84.6 | 8.7               | 28    | yes  | yes  | yes            | 16.3           | 16.1           | 22.4           | 12.6     |

<sup>a</sup> Abbreviations for columns Dec, Inc,  $\alpha_{95}$  Dir, K Dir, VGP Long, VGP Lat,  $\alpha_{95}$  VGP, and K VGP are as in Table 1. Fish Dir/Fish VGP indicate whether the distribution of the directional/VGP data is fisherian. O.G./O.A indicate whether the 95% confidence limits ( $\alpha_{95}$ ) of the mean direction/mean VGP overlap the GAD/Earth's rotation axis, respectively. Data of VGP scatter relative to the Earth's axis of rotation is given in columns S<sub>t</sub> (total scatter), S<sub>b</sub> (scatter corrected for within-site scatter), S<sub>u</sub> (upper 95% confidence limit of the scatter), and S<sub>l</sub> (lower 95% confidence limit of the scatter).

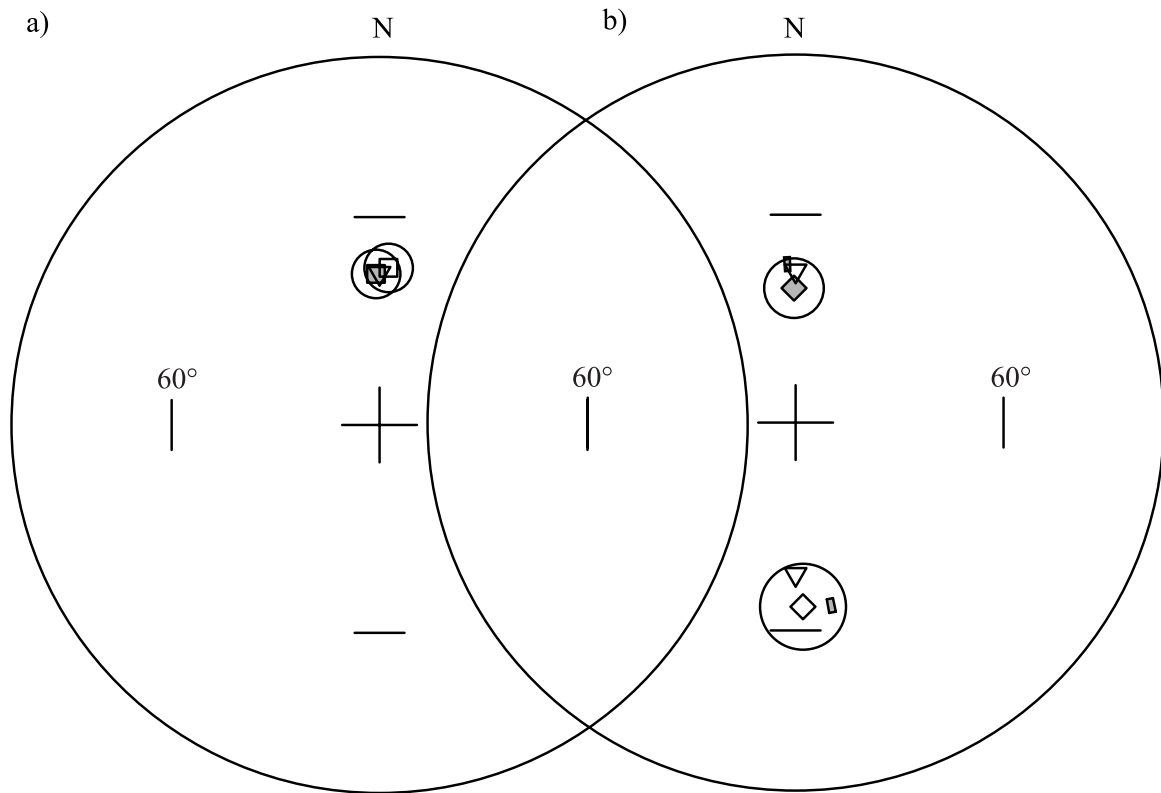


**Figure 6.** Equal area projection of mean directions from several groups of sites. (a) Comparison of the mean direction of the selected group of sites (shaded square) and the selected plus rejected group of sites (empty square) with the GAD (triangle pointing down). (b) Comparison of the mean direction from normal (gray-filled diamond) and reverse (empty diamond) data with the GAD (triangle pointing down) and ranges of inclination and declination in the area of study (shaded quadrilaterals) as modeled by *Johnson and Constable* [1995].

of the 53 sites that were studied. Excluding the sites that had Miocene ages or were likely to have that age, we calculated mean directions among 33 sites. The mean direction ( $D = 358.7^\circ$ ,  $I = -68.2^\circ$ ,  $\alpha_{95} = 3.5^\circ$ ) and mean VGP (Lat =  $88.5^\circ$ , Long =  $141.3^\circ$ ,  $\alpha_{95} = 5.4^\circ$ ) among the selected group of sites coincide at the 95% confidence level with the expected direction of the geocentric axial dipole (GAD) ( $\pm 68.1^\circ$ ) and axis of rotation respectively (Figures 4b and 6a and Table 3). Likewise the mean direction and mean VGPs among the normal, reverse and all the results (without consideration of selection criteria,  $N = 41$ ) coincide at the 95% confidence level with the GAD and axis of rotation respectively (Figures 4b and 6a and Table 3). The normal and reversed groups of sites pass the reversal test [*McFadden and McElhinny*, 1990] with a “B” classification. The VGP scatter with respect to the Earth’s axis of rotation (traditionally used as indicative of secular variation, Table 3) that

we obtained from the selected group of results is  $17.1^\circ$  (within-site scatter considered [e.g., *Johnson and Constable*, 1996]) with upper and lower 95% confidence limits of  $20.6^\circ$  and  $14.6^\circ$  [*Cox*, 1969]. This value is in close agreement with that predicted by Model G (*McFadden et al.*, 1988) of  $17.4^\circ$  (with upper and lower confidence limits of  $19.3^\circ$  and  $15.6^\circ$ ) for that latitude. Scatter values from high latitudes compatible with those expected from model G have been also recently obtained from lavas younger than 5 Ma of British Columbia [*Mejia et al.*, 2002], Deception Island [*Baraldo et al.*, 2003], and Possession Island [*Camps et al.*, 2001]. However, this has not been the case in the recent study from Patagonia (around  $47^\circ\text{S}$ ) by *Brown et al.* [2004] in which scatter is substantially higher than that expected from Model G.

[22] The IGRF of the year 2000 for the studied area is  $\text{Dec} = 13.5^\circ$  and  $\text{Inc} = -48.1^\circ$  and the GAD

for this same area is  $\text{Dec} = 0^\circ$ ,  $\text{Inc} = -68.1^\circ$ . Therefore the present inclination anomaly in the area is  $20^\circ$ . Such anomaly reflects the pronounced non-dipole structure of the present field in South America. The present inclination anomaly in the area of study is greater than the inclination anomaly of any of our sites that passed the selection criteria (Figure 3). This observation suggests that the present inclination anomaly is among the greatest that has occurred in the area at least during non-transitional states of the magnetic field.

[23] The mean directions of the normal and reverse data of this study were compared to ranges of directions corresponding to the declination and inclination anomalies (obtained mean values minus those expected from GAD) resulting from the TAF models (Figure 6b) obtained by JC95 for the past 5 Ma, that are based on normal (LN1 model) and reverse (LR1 model) data sets derived from lava flows [Johnson and Constable, 1996]. The agreement between the values modeled by JC95 for the Patagonia area and our results (Figure 6b) is facilitated by large 95% confidence ranges among our normal and reverse mean directions. However, the departure from the more ubiquitous negative and positive inclination anomalies (for normal and reverse data respectively) depicted in the TAF models of JC95 is not clearly observed in our data set. Only the inclination anomaly of  $-4.7^\circ$  ( $63.4^\circ$ – $68.1^\circ$ ) that we obtained from the reverse sites closely agrees with the  $-4^\circ$  to  $-6^\circ$  inclination anomaly range obtained for the Patagonia area by JC95. But at the same time, the declination anomaly of this same group of sites of  $\Delta D = -2.3^\circ$  ( $177.7^\circ$ – $180^\circ$ ) is quite distant from the range of  $-10^\circ$  to  $-12^\circ$  of the model. Detecting true departures from negative and positive inclination anomalies (for normal and reverse data respectively) would be important, because they would represent a contribution opposite to the axial quadrupole term (that causes the so-called far-sided effect seen in VGP plots [e.g., Wilson, 1970]) that is nevertheless expected to be small close to  $\pm 55^\circ$  latitudes such as in this study. Such axial quadrupole term ( $g_2^0$ ) contribution becomes zero at these latitudes because of the shape of the

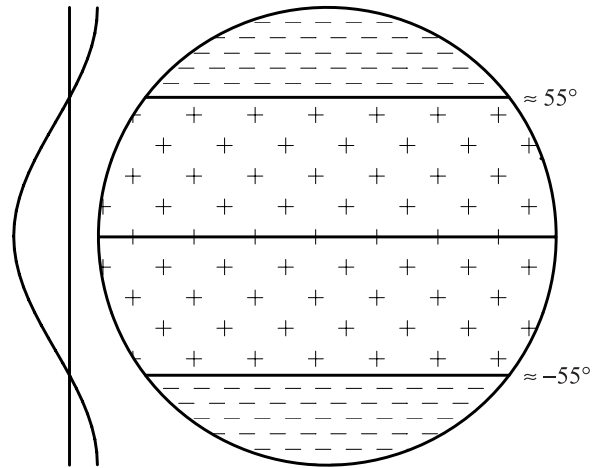


**Figure 7.** Form of the axial-quadrupole spherical harmonic term ( $g_2^0$ ). The contribution of this term, modulated entirely by the Legendre function, is 0 at  $\pm 55^\circ$  latitude.

wave of the Legendre polynomials of this spherical harmonic term (Figure 7).

## 8. Conclusions

[24] This paper presents high quality paleomagnetic results accompanied by precise new  $^{40}\text{Ar}/^{39}\text{Ar}$  geochronology from Pliocene-Pleistocene lavas from southern Patagonia. The fact that many rejected results coincide with greater departures from the GAD direction suggests that the selection criteria is adequate and highlights the need to apply stringent laboratory and data processing techniques such as those applied by Tauxe *et al.* [2000]. The mean direction and mean VGP presented closely follow and are consistent at the 95% confidence level with the GAD and axis of rotation respectively. Although the mean normal and mean reverse data sets presented indicate inclination and declination anomalies that are consistent at the 95% confidence level with those corresponding to the Patagonia area modeled by Johnson and Constable [1995], the departure from the far-sided effect indicated by those models is not suggested by our results. Rather, the overlap between our results and the modeled values occurs within a wide 95% confidence limit. Therefore the data presented do not reveal the presence of persistent non-dipole structures of the paleomagnetic field.

## Acknowledgments

[25] We wish to thank Miguel Haller, Massimo D’Orazio and Fabrizio Innocenti for the valuable information that they gave us about the geology of the studied area. We also want to thank Brian Jicha and Melissa Harper who did most of the sample preparation and isotopic measurements. This research was mostly supported by the National Science Foundation grant EAR-9804737 and partially supported by the Universidad de Buenos Aires grant TX19 (1999) and a graduate fellowship from the Florida Georgia Alliance for Minority Participation. Additionally,  $^{40}\text{Ar}/^{39}\text{Ar}$  dating was supported by National Science Foundation grants EAR-9909309 and EAR-014055 to Singer.

## References

- Baraldo, A., A. E. Rapalini, H. Boehnel, and M. Mena (2003), Paleomagnetic study of Deception Island, South Shetland Islands, Antarctica, *Geophys. J. Int.*, *153*, 333–343.
- Bird, J. (1938), Antiquity and migrations of the early inhabitants of Patagonia, *Geogr. Rev.*, *28*, 250–275.
- Brown, L. L., B. S. Singer, and M. L. Goring (2004), Paleomagnetism and  $^{40}\text{Ar}/^{39}\text{Ar}$  chronology of lavas from Meseta del Lago Buenos Aires, Patagonia, *Geochem. Geophys. Geosyst.*, *5*, Q01H04, doi:10.1029/2003GC000526.
- Camps, P., B. Henry, M. Prevot, and L. Faynot (2001), Geomagnetic paleosecular variation recorded in Plio-Pleistocene volcanic rocks from Possession Island (Crozet Archipelago, southern Indian Ocean), *J. Geophys. Res.*, *106*, 1961–1971.
- Cande, S. C., and D. Kent (1995), Revised calibration of the geomagnetic polarity time scale for the late Cretaceous and Cenozoic, *J. Geophys. Res.*, *100*, 6093–6095.
- Constable, C. G., C. L. Johnson, and S. P. Lund (2000), Global geomagnetic field models for the past 3000 years: Transient or permanent flux lobes?, *Philos. Trans. R. Soc. London, Ser. A*, *358*, 991–1008.
- Cox, A. (1969), Confidence limits of the precision parameter  $k$ , *Geophys. J. R. Astron. Soc.*, *18*, 545–549.
- Fisher, R. A. (1953), Dispersion on a sphere, *Proc. R. Soc. London, Ser. A*, *217*, 295–305.
- Fleck, R. J., J. H. Mercer, A. E. M. Nairn, and D. N. Peterson (1972), Chronology of the late Pliocene and early Pleistocene glacial and magnetic events in southern Argentina, *Earth Planet. Sci. Lett.*, *16*, 15–22.
- Jackson, A., A. R. T. Jonkers, and M. R. Walker (2000), Four centuries of geomagnetic secular variation from historical records, *Philos. Trans. R. Soc. London, Ser. A*, *358*, 957–990.
- Johnson, C. L., and C. G. Constable (1995), The time-averaged geomagnetic field as recorded by lava flows over the past 5 Myr, *Geophys. J. Int.*, *122*, 489–519.
- Johnson, C. L., and C. G. Constable (1996), Paleosecular variations recorded by lava flows over the past five million years, *Philos. Trans. R. Soc. London, Ser. A*, *354*, 89–141.
- Kirschvink, J. L. (1980), The least squares line and plane and the analysis of palaeomagnetic data, *Geophys. J. R. Astron. Soc.*, *62*, 699–718.
- Lee, S. (1983), A study of the time-averaged paleomagnetic field for the last 195 million years, Ph.D. thesis, Aust. Natl. Univ., Canberra, Australia.
- Love, J. J. (2000), On the anisotropy of secular variation deduced from paleomagnetic volcanic data, *J. Geophys. Res.*, *105*, 5799–5816.
- McElhinny, M. W., and P. L. McFadden (1997), Paleosecular variation over the past 5 Myr based on a new generalized database, *Geophys. J. Int.*, *131*, 240–252.
- McFadden, P. L., and M. W. McElhinny (1990), Classification of the reversal test in paleomagnetism, *Geophys. J. Int.*, *103*, 725–729.
- McFadden, P. L., R. T. Merrill, and M. W. McElhinny (1988), Dipole/quadrupole family modeling of paleosecular variation, *J. Geophys. Res.*, *93*, 1583–1588.
- Meglioli, A. (1992), Glacial geology and chronology of southernmost Patagonia and Tierra del Fuego, Argentina and Chile, Ph.D. thesis, Lehigh Univ., Bethlehem, Penn.
- Mejia, V., R. W. Barendregt, and N. D. Opdyke (2002), Paleosecular variation of Brunhes age lava flows from British Columbia, Canada, *Geochem. Geophys. Geosyst.*, *3*(12), doi:10.1029/2002GC000353.
- Mercer, J. H. (1976), Glacial history of southernmost South America, *Quat. Res.*, *6*, 125–166.
- Quidelleur, X., J. P. Valet, V. Courtillot, and G. Hulot (1994), Long-term geometry of the geomagnetic field for the last five million years: An updated secular variation database, *Geophys. Res. Lett.*, *21*, 1639–1642.
- Ramos, V. A., and S. M. Kay (1992), Southern Patagonian plateau basalts and deformation: Backarc testimony of ridge collisions, *Tectonophysics*, *205*, 261–282.
- Renne, P. R., C. C. Swisher, A. L. Deino, D. B. Karner, T. L. Owens, and D. J. DePaolo (1998), Intercalibration of standards, absolute ages and uncertainties in  $^{40}\text{Ar}/^{39}\text{Ar}$  dating, *Chem. Geol.*, *145*, 117–152.
- Singer, B. S., K. A. Hoffman, A. Chauvin, R. S. Coe, and M. S. Pringle (1999), Dating transitionally magnetized lavas of the late Matuyama Chron: Toward a new  $^{40}\text{Ar}/^{39}\text{Ar}$  timescale of reversals and events, *J. Geophys. Res.*, *104*, 679–693.
- Singer, B. S., M. K. Relle, K. A. Hoffman, A. Battle, C. Laj, H. Guillou, and J. C. Carracedo (2002), Ar/Ar ages from transitionally magnetized lavas on La Palma, Canary Islands, and the geomagnetic instability timescale, *J. Geophys. Res.*, *107*(B11), doi:10.1029/2001JB001613.
- Singer, B. S., R. J. Ackert, and H. Guillou (2004),  $^{40}\text{Ar}/^{39}\text{Ar}$  and K-Ar chronology of Pleistocene glaciations in Patagonia, *Geol. Soc. Am. Bull.*, in press.
- Skewes, M. A., and C. R. Stern (1979), Petrology and geochemistry of alkali basalts and ultramafic inclusions from the



- Palei-Aike volcanic field in southern Chile and the origin of the Patagonian plateau lavas, *J. Volcanol. Geotherm. Res.*, *6*, 3–25.
- Szeremeta, N., C. Laj, H. Guillou, C. Kissel, A. Zamaud, and J. C. Carracedo (1999), Geomagnetic paleosecular variation in the Brunhes period, from the island of El Hierro (Canary Islands), *Earth Planet. Sci. Lett.*, *165*, 241–253.
- Tauxe, L., H. Staudigel, and J. R. Wijbrans (2000), Paleomagnetism and  $^{40}\text{Ar}/^{39}\text{Ar}$  ages from La Palma in the Canary Islands, *Geochem. Geophys. Geosyst.*, *1*, paper 2000GC000063.
- Wilson, R. L. (1970), Permanent aspects of the Earth's non-dipole magnetic field over Upper Tertiary times, *Geophys. J. R. Astron. Soc.*, *19*, 417–437.